October 2008

Control of strain relaxation in tensile and compressive oxide thin films

Yudi Wang
University of Pennsylvania

Soo Gil Kim
University of Pennsylvania

I-Wei Chen
University of Pennsylvania, iweichen@seas.upenn.edu

Postprint version. Published in *Acta Materialia*, Volume 56, Issue 18, October 2008, pages 5312-5321.
Publisher URL: http://dx.doi.org/10.1016/j.actamat.2008.07.010

Control of strain relaxation in tensile and compressive oxide thin films

Abstract
Tensile and compressive solid-solution thin films based on $LaAlO_3$ and $CaZrO_3$ compositions were grown on perovskite oxide substrates using pulsed laser deposition to study growth mode transitions and strain relaxation. A buried layer of $SrRuO_3$ between the thin film and the $SrTiO_3$ substrate was also introduced to provide an auxiliary embedded strain gauge, which helps identify the critical conditions for the onset of catastrophic strain relaxation events – cracking and dislocation cascades. The results are compared with theoretical predictions to provide guidelines on some general deposition conditions that may be used to obtain smooth, crystalline and defect-free thin films of interest to perovskite-based heterostructures.

Keywords
dislocation, fracture, multilayer thin films, perovskites, laser deposition

Comments
Postprint version. Published in *Acta Materialia*, Volume 56, Issue 18, October 2008, pages 5312-5321.
Publisher URL: http://dx.doi.org/10.1016/j.actamat.2008.07.010

Available online at www.sciencedirect.com
ScienceDirect
Acta Materialia xxx (2008) xxx–xxx
Acta MATERIALIA
www.elsevier.com/locate/actamat

Control of strain relaxation in tensile and compressive oxide thin films

Yudi Wang, Soo Gil Kim, I-Wei Chen *

Department of Materials Science and Engineering, University of Pennsylvania, 3231 Walnut Street, Philadelphia, PA 19104-6272, USA

Received 13 March 2008; received in revised form 19 June 2008; accepted 7 July 2008

Abstract

Tensile and compressive solid-solution thin films based on $LaAlO_3$ and $CaZrO_3$ compositions were grown on perovskite oxide substrates using pulsed laser deposition to study growth mode transitions and strain relaxation. A buried layer of $SrRuO_3$ between the thin film and the $SrTiO_3$ substrate was also introduced to provide an auxiliary embedded strain gauge, which helps identify the critical conditions for the onset of catastrophic strain relaxation events – cracking and dislocation cascades. The results are compared with theoretical predictions to provide guidelines on some general deposition conditions that may be used to obtain smooth, crystalline and defect-free thin films of interest to perovskite-based heterostructures.

Keywords: Dislocation; Fracture; Multilayer thin films; Perovskites; Laser deposition

1. Introduction

Oxide thin film devices such as dielectrics, ferroelectrics, magnetics and resistance memories typically contain at least one functionally active layer resting on a bottom electrode layer, which is in turn supported on a substrate [1]. In these multilayer heterostructures, it is important to maintain flatness in every layer. To achieve this, catastrophic strain relaxation events such as cracking [2–6] or threading dislocation cascades [7–12] must be avoided. Of considerable interest among oxide devices are those built upon an ABO_3 perovskite platform since perovskite members, regardless of their myriad of functional properties, share a common crystal structure with similar lattice parameters. This led us to investigate two model all-perovskite heterostructures, one with tensile overlayers and the other with compressive overlayers, both built on a common platform consisting of a bottom electrode ($SrRuO_3$) and a single-crystal substrate ($SrTiO_3$). The goal is to characterize and compare their relaxation behaviors and, in so doing, identify favorable conditions for growing atomically flat overlayers.

Since oxide processing typically involves high temperature, a film/substrate mismatch in either lattice parameter or thermal expansion coefficient can lead to a residual strain in the film. To simplify the problem without losing generality, we selected two systems in which the lattice mismatches are so large (about ±2.7%) that the thermal mismatch may be ignored. They are $LaAlO_3$-based tensile overlayers which exhibit cracking and $CaZrO_3$-based compressive overlayers which exhibit dislocation cascades (called cross-hatches). These strain relaxation mechanisms are common for many oxide thin films [5–8], so our comparative study of their occurrence should be of general interest. In practice, although the end members $LaAlO_3$ and $CaZrO_3$ have different magnitude of misfit strains, we can use two solid solutions based on these end members to equalize the strain magnitude. Moreover, by incorporating a mismatched buried layer ($SrRuO_3$) that is initially clamped to the substrate, we have built in a sensitive "strain gauge" capable of reporting the progression of strain relaxation in the overlayer layer [13]. Since the mismatch between the buried layer and the substrate ($SrTiO_3$) is relatively small (about 0.64%), a tension/compression symmetry approximately holds in these model systems.

* Corresponding author.
E-mail address: iweichen@seas.upenn.edu (I-Wei Chen).

1359-6454/$34.00 © 2008 Acta Materialia Inc. Published by Elsevier Ltd. All rights reserved.
doi:10.1016/j.actamat.2008.07.010

Theoretically, the critical condition for crack formation is expressed in terms of critical strain energy which scales with the film thickness and the in-plane strain [14]. Likewise, the critical condition for cross-hatch formation is expressed in terms of critical glide force (on dislocation), which also scales with the thickness and strain [15]. These considerations will guide the presentation of our data on overlayers of different thickness and strain. As is well known in thin film research, the strain state can be greatly influenced by the deposition condition, especially that for the first few atomic layers [16]. Therefore, we have also systematically examined the interplay between the growth modes, strain evolution and the onset of the catastrophic strain relaxation events in our model systems.

2. Methods

2.1. Materials and experimental procedures

To simulate the construct of a typical all-perovskite architecture, we used $SrRuO_3$ (30 nm thick) as the "bottom electrode" and $SrTiO_3$ (100 single crystal) as the substrate. Relative to the cubic $SrTiO_3$ (lattice constant $a = 0.3905$ nm) in the 100 direction, rhombohedral $LaAlO_3$ (pseudocubic $a = 0.3790$ nm) [17] has a tensile mismatch of 3.03% while orthorhombic $CaZrO_3$ (pseudocubic $a = 0.4012$ nm) [18] has a compressive mismatch of 2.67%. We used a solid solution of 90 at.% $LaAlO_3$ and 10 at.% $LaNiO_3$ (pseudocubic $a = 0.3830$ nm) [19] to reach an estimated tensile mismatch of 2.79%; this composition will be referred to as LAO. Likewise, we used a solid solution of 94.5 at.% $CaZrO_3$ and 5.5 at.% $SrRuO_3$ (pseudocubic $a = 0.3930$ nm) [20] to reach an estimated compressive mismatch of 2.57%; this composition will be referred to as CZO.

The substrate was prepared using a variation of the standard technique [21,22] to obtain atomically flat TiO_2-terminated 100 surface, which has a step-terrace structure with unit-cell-height (0.4 nm) step edges without any surface defects. $SrRuO_3$ was deposited at 700 °C under 100 mTorr oxygen pressure using a dense $SrRuO_3$ target and a pulsed laser (wavelength = 248 nm, 10 Hz, 200 mJ/pulse) at a rate of 0.011 nm/pulse. Because of the relatively small misfit (0.64%), $SrRuO_3$ is completely clamped by the substrate following a pseudo-tetragonal lattice correspondence with an out-of-plane lattice parameter of 0.3958 nm that is thickness-independent. The surface roughness measured by an atomic force microscope (AFM, Nanoscope IIIA Dimension 3100, Digital Instrument, Santa Barbara, CA) was 0.18 nm over a scanned area of 2 × 2 μm. This film was stable (without change in surface morphology or diffraction pattern) during post-deposition annealing (1 h) at 650 °C at an oxygen pressure from 10^{-3} to 10^{2} mTorr. Details of the above procedures are available elsewhere [23].

The overlayers were also deposited by pulsed laser deposition (PLD) using two targets ($LaAlO_3$ and $LaNiO_3$ for LAO; $CaZrO_3$ and $SrRuO_3$ for CZO) which were ablated at an appropriate laser-hit ratio set by referring to the calibration data of single-target deposition rates under the same deposition condition (see Table 1 for representative deposition rates for single targets). The deposition temperature, oxygen pressure and film thickness were systematically varied to obtain overlayers of different characteristics. Film structure was analyzed using high-resolution X-ray diffraction (HXRD), performed on a four-circle diffractometer (D8 Discover, Bruker-AXS, Madison, WI) with a Cu $K\alpha_1$ source selected by a four-bounce Ge 220 asymmetric monochromator, yielding 2θ–ω and ω rocking-curve scans. Film thickness was also measured by X-ray reflectivity using the same instrument. Film morphology and statistics of surface features (crack spacing over 10 × 10 μm, cross-hatch spacing over 2 × 2 μm) were examined using AFM.

Table 1
Representative deposition rates per pulsed laser shot (200 mJ) on 100 $SrTiO_3$ using a single target

Target	Deposition conditions	Deposition rate (nm/shot @ 200 mJ)
$SrRuO_3$	600 °C–50 mTorr	0.0112
$CaZrO_3$	600 °C–50 mTorr	0.0166
$LaAlO_3$	600 °C–1 mTorr	0.0127
$LaNiO_3$	600 °C–1 mTorr	0.0146

2.2. Theoretical considerations

In an elastically isotropic solid, the in-plane strain ε is related to the out-of-plane strain ε' by $\varepsilon' = -2\nu\varepsilon/(1-\nu)$, which reduces to $\varepsilon = -\varepsilon'$ when Poisson's ratio ν is 1/3. Since this is a reasonable value for most oxides, we will use $\varepsilon = -\varepsilon'$ to compute the in-plane strain from the HXRD data of the out-of-plane lattice spacing.

The critical thickness for crack formation in a biaxially stretched tensile film is given by the crack propagation condition balancing elastic energy release and the work of fracture W_f. If the film and the substrate have the same elastic constants, the critical thickness is [14]

$$h_c = \frac{0.5W_f(1-\nu)}{(1+\nu)E\varepsilon^2} \quad (1)$$

where E is Young's modulus. The product of film thickness and in-plane tensile strain (squared) thus emerges as the parameter to be used to locate the critical cracking condition. The $SrRuO_3$ buried layer need not be considered since it is under compression.

The critical thickness for cross-hatch formation is taken as that required for propagating a threading dislocation. Extending the method of Freund [9,24], we have previously found the driving force f for threading-dislocation advance ($f = 0$ being the critical condition) to be [13]

$$f = 2Gb(h_o\varepsilon_o + h_b\varepsilon_b)\sin\lambda\sin\beta\left(\tfrac{1+\nu}{1-\nu}\right) - \frac{Gb^2\sin^2\beta}{4\pi(1-\nu)}\left[\frac{(1-\nu\cos^2\beta)}{\sin^2\beta}\ln\left(\frac{2(h_o+h_b)}{r_o}\right) - \tfrac{1}{2}\cos 2\lambda - \tfrac{1-2\nu}{4(1-\nu)}\right] \quad (2)$$

Please cite this article in press as: Wang Y et al., Control of strain relaxation in tensile and compressive oxide thin films, Acta Mater (2008), doi:10.1016/j.actamat.2008.07.010

for an overlayer (o)/buried-layer (b)/substrate system with identical ν and shear modulus G. In the above, the misfit forces due to the overlayer ($\alpha h_o \varepsilon_o$) and the buried layer ($\alpha h_b \varepsilon_b$) are countered by the self force of a dislocation of a Burgers vector b with a core radius r_o ($r_o \sim b/4$), inclined at angles β (between the Burgers vector and the slip plane/substrate intersection) and λ (between the slip plane and the film normal). For perovskite oxides, the dominant dislocation system is <110> {110} [10,11] with $b = 0.5523$ nm, hence $\beta = 90°$ and $\lambda = 45°$ for a (001) oriented film. The product of film thickness and in-plane tensile strain thus emerges as the parameter to be used to identify the critical cross-hatching condition.

3. Results

3.1. $LAO/SrRuO_3/SrTiO_3$ system

3.1.1. Critical strain/thickness

Cracks were observed in LAO overlayers deposited at 600 °C under 100 mTorr of oxygen. Under this condition, the critical thickness is between 2.5 nm (without crack) and 5 nm (with one crack) as shown in the AFM height images in Fig. 1. The crack spacing rapidly decreases with overlayer thickness, reaching a saturation spacing of 0.5 μm at a large thickness. These overlayers have the same tensile strain of about 1.4% independent of layer thickness, even after cracking. To delineate the critical cracking condition, we plot in Fig. 2 the film thickness h and squared tensile strain ε^2 of the LAO films deposited under various temperature/pressure conditions. A sharp boundary separating cracked and uncracked films is evident from the plot. This boundary also holds for the (unpublished) data of 90 at.% $LaAlO_3$–10 at.% $SrRuO_3$ films which in the unstrained state have a similar estimated lattice parameter. It is clear that under such a large tensile misfit strain (2.79%), cracking would be very difficult to avoid at any reasonable thickness.

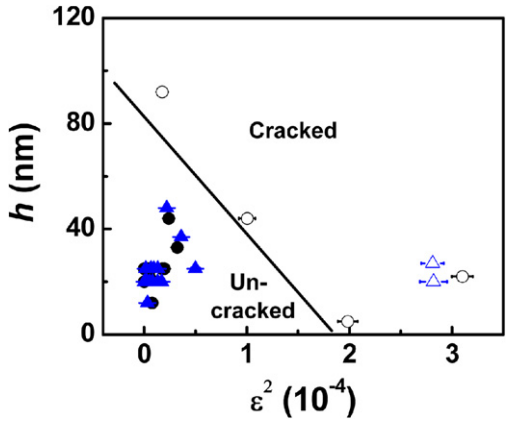

Fig. 2. Crack occurrence vs. thickness and strain in LAO (circles) and 90 at.% $LaAlO_3$–10 at.% $SrRuO_3$ (triangles) overlayers deposited under various conditions. Open symbols for cracked layers; filled symbols for uncracked layers.

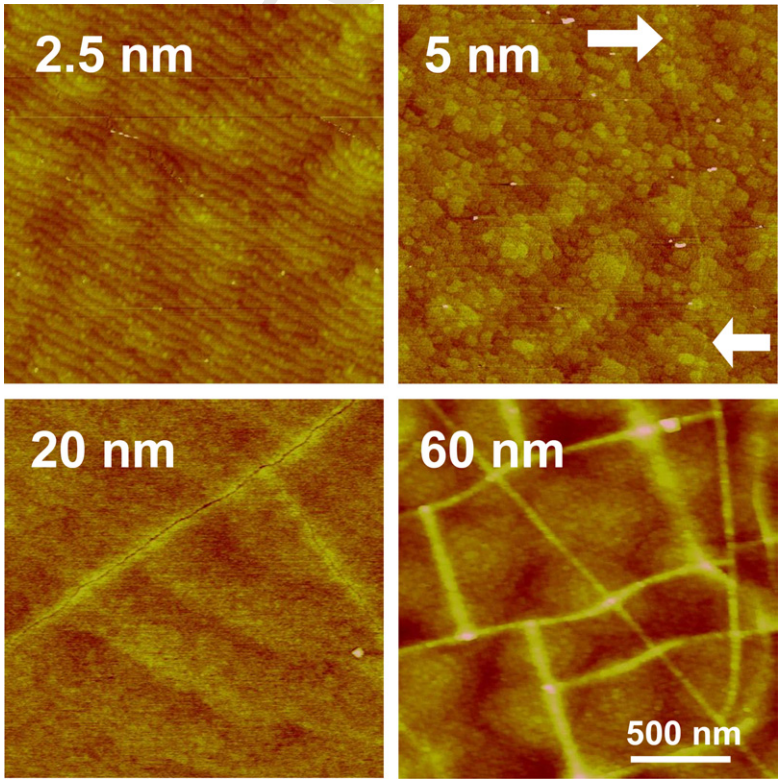

Fig. 1. Surface morphology of LAO layers of 2.5–60 nm thick deposited at 600 °C with 100 mTorr oxygen. Arrows indicate a crack in the 5 nm film.

Please cite this article in press as: Wang Y et al., Control of strain relaxation in tensile and compressive oxide thin films, Acta Mater (2008), doi:10.1016/j.actamat.2008.07.010

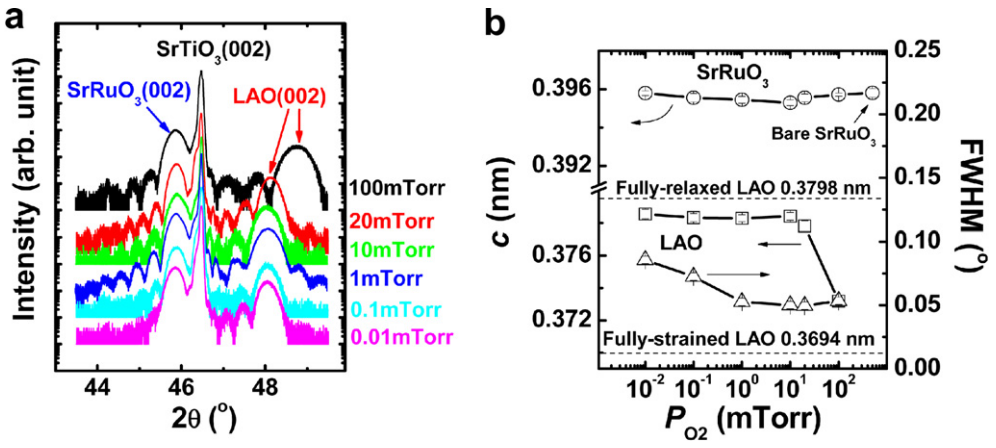

Fig. 3. (a) Profiles of 2θ–ω scans of films deposited at 600 °C under various oxygen pressures as labeled. (b) Effect of deposition pressure on out-of-plane lattice parameters of LAO and $SrRuO_3$ layers and FWHM of rocking curve of LAO layers. Note abrupt right shift of LAO peak in (a).

3.1.2. Strain evolution

Most of the LAO overlayers deposited at a temperature from 550 to 700 °C under an oxygen pressure from 10^{-2} mTorr to above 10 mTorr are in a similar state of strain, typically much less than 1%. However, the films deposited at 100 mTorr have a strain of 1.8% as illustrated in Fig. 3, which plots the 2θ–ω scans and lattice parameters of the 20 nm overlayers deposited at 600 °C under various pressures. Their AFM height images in Fig. 4a–d show cracking in the 100 mTorr film only. It is also notable from Fig. 3a that the buried $SrRuO_3$ films are in the same strain state whether the LAO overlayer is cracked or not; indeed the strain state of $SrRuO_3$ is essentially the same as that before LAO deposition.

3.1.3. Growth modes

All the films described above have a similar surface roughness when they are thicker than 5 nm. This is already apparent from AFM height images in Fig. 4a–d which indicate all the overlayers grew in a step-flow manner. Additional AFM height images are shown in Fig. 4e–f for a series of 20 nm thick LAO films deposited at 1 mTorr at

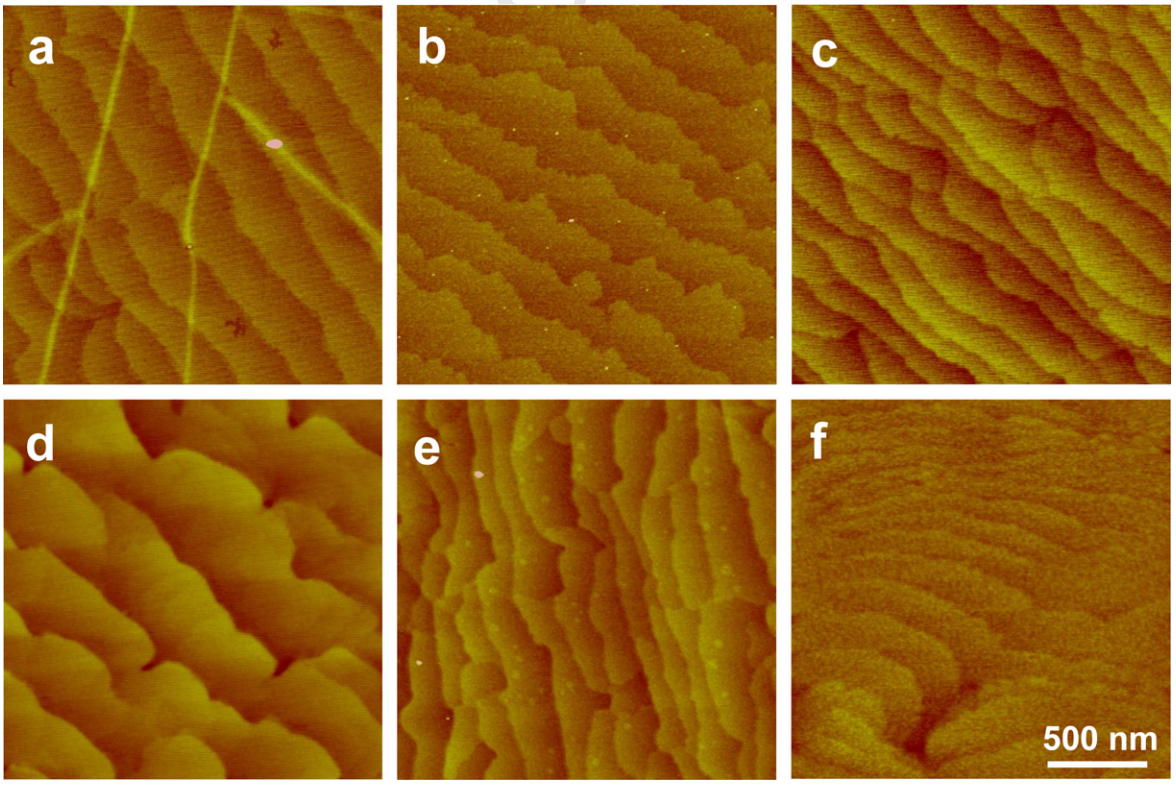

Fig. 4. Surface morphology of 20 nm LAO films deposited at 600 °C under various oxygen pressures: (a) 100 mTorr; (b) 20 mTorr; (c) 1 mTorr; (d) 0.1 mTorr; and with 1 mTorr oxygen pressure at (e) 550 °C; and (f) 700 °C.

Please cite this article in press as: Wang Y et al., Control of strain relaxation in tensile and compressive oxide thin films, Acta Mater (2008), doi:10.1016/j.actamat.2008.07.010

temperatures from 550 to 700 °C. The films grew in the step-flow mode with a clear step-terrace structure at 600 to 700 °C (Fig. 4f), and in the layer-by-layer mode at 550 °C (Fig. 4e), which contains some isolated islands on the smooth terraces. Hereafter, we will often refer to step-flow mode and layer-by-layer mode as 2D growth mode, in which terraces are common and islands are unit-cell high. Beyond a certain thickness, the LAO overlayers all grew in the 2D mode.

3.1.4. Initial growth and its pressure dependence

The origin of the pressure effect on the strain state of the LAO overlayer may lie in the initial growth since thicker overlayers apparently have a similar morphology. To investigate this possibility, LAO overlayers of a few monolayer (ML) thick were deposited at 600 °C under different oxygen pressures. As shown in Fig. 5a–d for the overlayers grown under 1 mTorr oxygen, the initial LAO islands are very small and randomly distributed covering less than 1 ML (Fig. 5b) of the $SrRuO_3$ terraces. At 1.5 ML (Fig. 5c), some of the islands are 2 unit-cell (0.8 nm) high but part of the $SrRuO_3$ surface remains uncovered, indicating that at 1 mTorr the initial growth of LAO on $SrRuO_3$ is an island process. (Hereafter, we will often refer to island mode as 3D mode. Generally, islands in the 3D mode are more than one unit-cell high.) When the film is 6 ML thick (Fig. 5d), there is no more bare $SrRuO_3$ surface, but many isolated islands can still be seen on the terraces although they are now larger in size than before (e.g. Fig. 5b). With further deposition, fewer islands are found and by 15 ML (Fig. 5a inset), the film already grew in the layer-by-layer mode. In contrast, the surface morphologies of films deposited under 100 mTorr oxygen are shown in Fig. 5e and f, which follow a similar evolution but the island sizes are much larger at a comparable overlayer thickness (cf. Fig. 5c and e). Once the thickness reaches 6 ML (Fig. 5d and f), the surface morphologies with different pressures appear similar. This indicates that the island size of the first few ML before the 3D/2D mode transition is probably critical for (tensile) strain transfer: smaller islands transfer less while larger islands transfer more.

Lastly, we mention that LAO overlayers grown at 500 °C at 1 mTorr are very smooth but not crystallized.

3.2. $CZO/SrRuO_3/SrTiO_3$

3.2.1. Growth modes and cross-hatch

Overlayers of 20 nm thick CZO deposited under various temperatures and pressures as marked in Fig. 6 exhibit a systematic trend toward cross-hatch formation (indicated by crosses) and growth mode transition (indicated by the

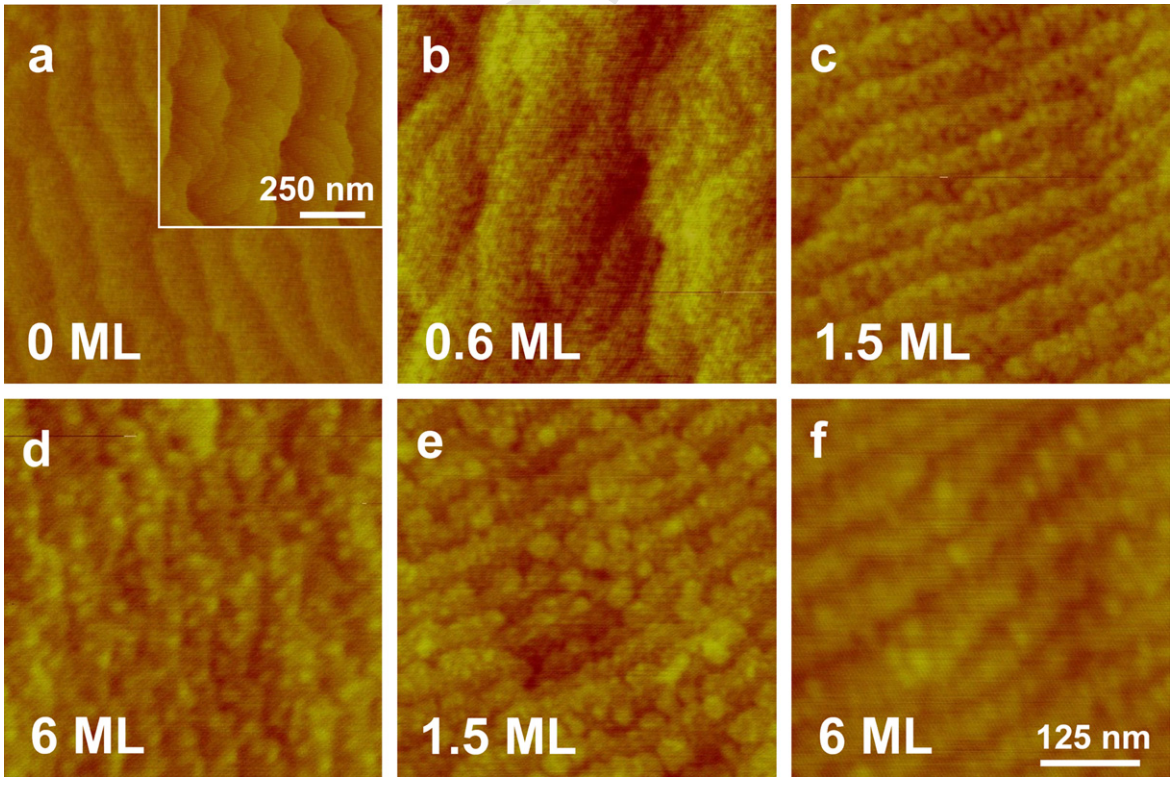

Fig. 5. Surface morphology of LAO films of various thickness in monolayer (ML) deposited at 600 °C; (a–d) with 1 mTorr oxygen; and (e–f) with 100 mTorr oxygen. Inset in (a) is 15 ML LAO film with 1 mTorr oxygen.

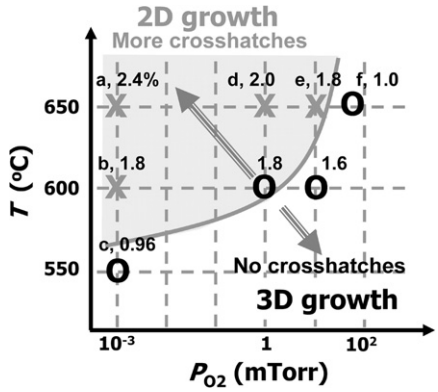

Fig. 6. Summary of deposition conditions (temperature and P_{O_2}, growth modes (2D vs. 3D) and in-plane compressive strain (shown as number next to symbol, in %) for CZO overlayers with (crosses) and without (circles) cross-hatch. Alphabetical labels used here are the same as in Figs. 7 and 10.

2D/3D boundary). Here the growth mode is identified by referring to the AFM images in Fig. 7 for the films that are alphabetically labeled in the same ways as in Fig. 6. The growth mode progresses from step-flow (a and d), to layer-by-layer (b), to island (c and f) growth (small isolated islands on smooth terraces can also be seen in the layer-by-layer mode (b), indicating some 3D-mode contribution). In the intermediate state (e), the growth mode lies between 2D and 3D as evidenced by the clear step-terrace structure (presumably inherited from the $SrRuO_3$ buried layer, indicative of the 2D mode) together with smooth tiny islands (indicative of the 3D mode) forming on the flat terrace. In the above, film f illustrates the very smooth, cross-hatch-free surface that is possible when the 3D mode just becomes dominant. Further into the 3D mode territory (e.g., at 650 °C and 100 mTorr, to the right of f in Fig. 6) both the island size and the film roughness increase. Comparing the cross-hatch occurrence with the growth mode, it becomes apparent that cross-hatch forms only in 2D growth; the further into the 2D growth territory, the more numerous the cross-hatches. Film a has the highest density of cross-hatches with a spacing of about 118 nm. These cross-hatches have surface traces (1–3 nm high) aligned along two equivalent <100> directions according to X-ray diffraction. Such trace direction is consistent with the dominant slip system <110> {110} in perovskite structured materials.

Lastly, we note that CZO overlayers grown at slightly below 550 °C at 10^{-3} mTorr are not crystallized.

3.2.2. Critical conditions for cross-hatch formation

We determined the critical thickness for cross-hatching using a set of CZO overlayers deposited at 650 °C under 1 mTorr oxygen pressure, which is well inside the 2D growth territory according to Fig. 6. Indeed, the films grew in the step-flow mode with a clear step-terrace structure as verified in Fig. 8. In the 5 nm thick film cross-hatches were not observed, at 10 nm they are clearly visible and with a

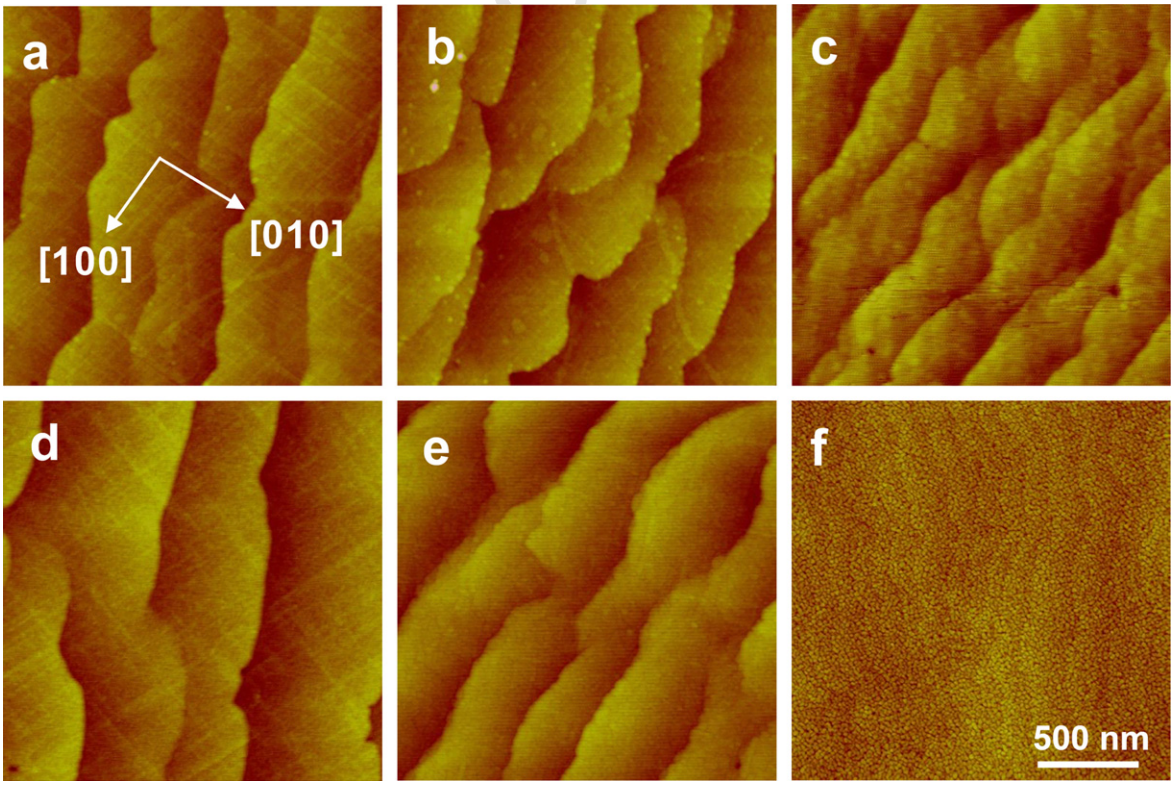

Fig. 7. Surface morphology of 20 nm CZO overlayers deposited under various conditions alphabetically labeled in the same way as in Fig. 6. (a) 650 °C–0.001 mTorr; (b) 600 °C–0.001 mTorr; (c) 550 °C–0.001 mTorr; (d) 650 °C–1 mTorr; (e) 650 °C–10 mTorr; (f) 650 °C–50 mTorr.

Please cite this article in press as: Wang Y et al., Control of strain relaxation in tensile and compressive oxide thin films, Acta Mater (2008), doi:10.1016/j.actamat.2008.07.010

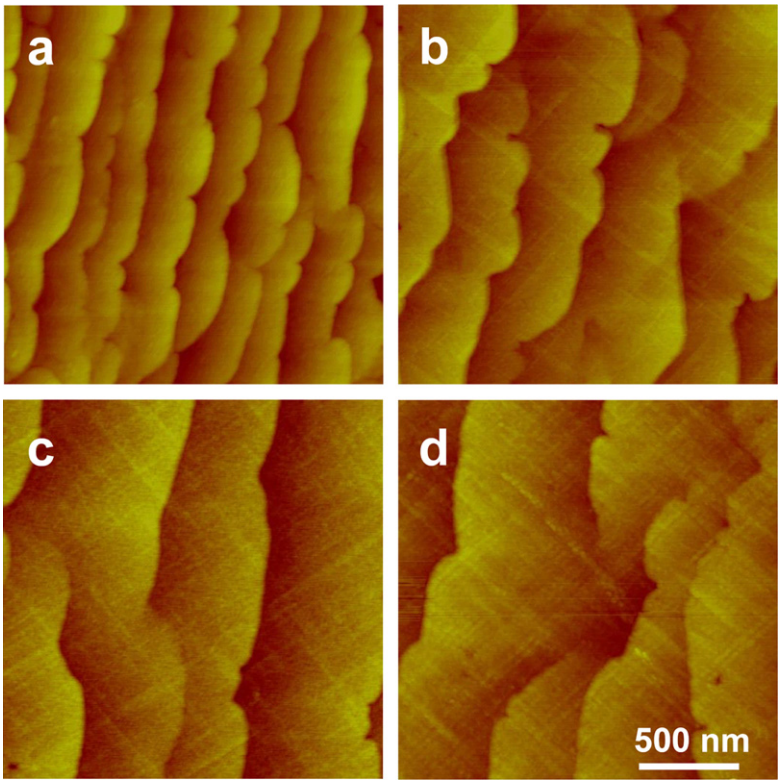

Fig. 8. Thickness effect on surface morphology of CZO overlayers deposited at 650 °C with 1 mTorr oxygen: (a) 5 nm; (b) 10 nm; (c) 20 nm; (d) 30 nm.

further increase in thickness their spacing decreases, from 218 nm in Fig. 8b to 120 nm in Fig. 8d. The critical thickness is placed between 5 and 10 nm in this case.

The 2θ–ω scan curves in Fig. 9a show a progressive decrease in the out-of-plane lattice parameters in the CZO overlayer as the thickness increases, indicating expansion of the in-plane lattice parameter, i.e., a relief of the in-plane compression. The $SrRuO_3$ buried layer is also relaxed in the same direction: without any CZO overlayer, the $SrRuO_3$ (002) peak is clearly distinct from that of the $SrTiO_3$ substrate; with a growing CZO overlayer the peak moves to a higher angle merging with the substrate peak. The computed in-plane compressive strains are shown in Fig. 9b. Beyond a critical thickness the strain in CZO relaxes from 2.5% to 2.0%; in $SrRuO_3$ it relaxes from 0.6% to 0.2%. Therefore, both layers relax by a similar magnitude.

Lattice parameters were similarly determined for the films shown in Fig. 6 using HXRD (data not shown [23]). As mentioned in Section 2.2, in an elastically isotropic solid, the in-plane strain ε is related to the out-of-plane strain ε' by $\varepsilon' = -2\nu\varepsilon/(1-\nu)$, which reduces to $\varepsilon = -\varepsilon'$

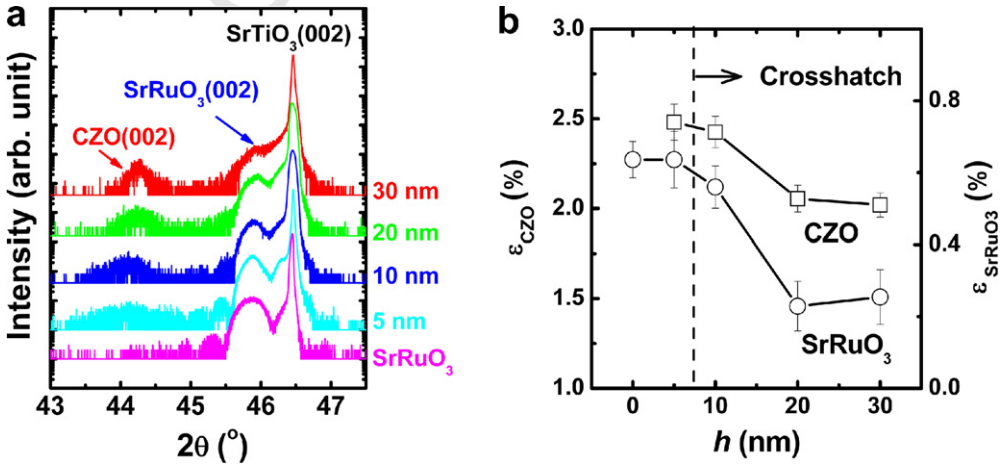

Fig. 9. (a) Profiles of 2θ–ω scans of CZO films with various thickness as labeled; (b) thickness dependence of compressive in-plane strain in CZO and $SrRuO_3$ layers.

Please cite this article in press as: Wang Y et al., Control of strain relaxation in tensile and compressive oxide thin films, Acta Mater (2008), doi:10.1016/j.actamat.2008.07.010

when Poisson's ratio ν is 1/3. Since this is a reasonable value for most oxides, we will use $\varepsilon = \hat{\varepsilon}'$. Therefore, the in-plane strain may be immediately obtained from the HXRD data of the out-of-plane lattice spacing. The in-plane compressive strains of the CZO overlayers thus computed are given as numbers next to the symbols in Fig. 6. Clearly, the highest in-plane strain is in film a in which cross-hatches are most numerous. This may seem surprising since there should be more strain relaxation with more numerous cross-hatches, as indicated in Fig. 9. However, the initial strains built up in different growth modes are different, being larger in 2D growth and smaller in 3D growth. Moreover, in the overlayer the maximum strain relaxation due to cross-hatching appears limited to 0.5% according to Fig. 9 in which the same initial strain is maintained by using the same growth condition, hence the growth mode. Therefore, the different strain levels shown in Fig. 6 primarily reflect the different initial strain before relaxation. Across the 3D (without cross-hatch)/2D (with cross-hatches) boundary the CZO strain abruptly increases from about 1% to about 1.8% for these 20 nm overlayers. Taking into account the relaxation strain of 0.5% due to cross-hatching, we estimate the discontinuity in the initial strain across the boundary is about 1.3%. Meanwhile, there is obvious strain relaxation in the $SrRuO_3$ buried layer, plotted in Fig. 10 for the same set of films alphabetically labeled as in Figs. 6 and 7. Here in the buried layer strain relaxation increases with increasing cross-hatching.

4. Discussion

4.1. Growth modes and surface polarity of oxide films

The transition from 3D growth to 2D growth delineated in Fig. 6 for CZO overlayers is actually general for PLD: 2D growth at higher temperature and/or lower pressure; 3D growth at lower temperature and/or higher pressure. This is illustrated by retracing the 2D/3D boundary for CZO in Fig. 11. In the figure we also outlined the growth modes/crystallization thresholds for LAO and $SrRuO_3$ (grown on $SrTiO_3$, from Ref. [23]) films at a comparable thickness of about 20 nm. Note that for both LAO and $SrRuO_3$, only 2D growth was observed for the entire range of conditions mapped in Fig. 11 (550–700 °C and 10^{-3}–10^{2} mTorr) once their crystallization thresholds are exceeded. Note further that the crystallization thresholds for LAO and $SrRuO_3$ are lower than that of CZO. This correlation strongly suggests that the more complete dominance of 2D growth in LAO and $SrRuO_3$ is likely to be related to their faster kinetics, and that the 3D/2D growth transition in CZO is enabled by faster kinetics. This seems reasonable since in PLD a lower pressure allows the ablated atoms to maintain a higher kinetic energy, which would correspond to a higher temperature.

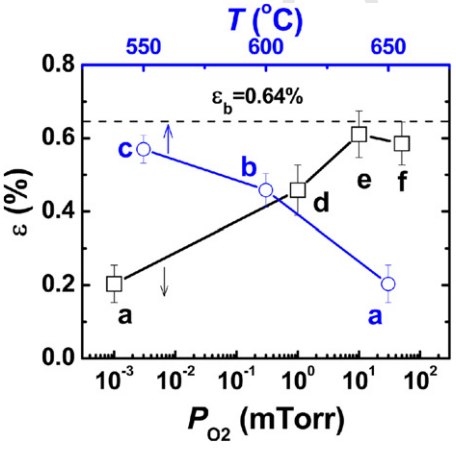

Fig. 10. Dependence of compressive in-plane strain in $SrRuO_3$ buried layer on deposition temperature (with $P_{O_2} = 10^{-3}$ mTorr) and pressure (with $T = 650$ °C). Samples alphabetically labeled in the same way as in Figs. 6 and 7.

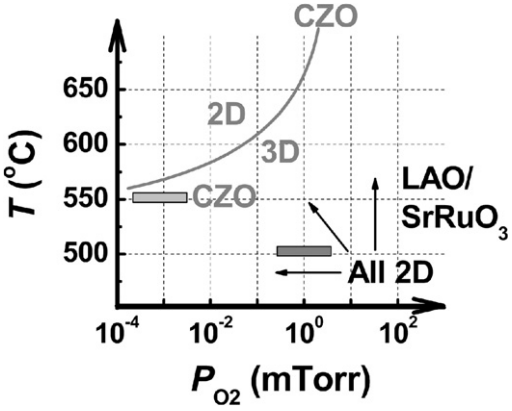

Fig. 11. 2D/3D growth mode transition for three oxides on $SrTiO_3$ (001) substrate. Bars indicate crystallization thresholds.

The above comparison is valid for thicker films. In oxide systems, the initial film growth at a different composition from the substrate could be extremely sensitive to the chemical nature of the atomic layer [25,26]. In particular, the surface polarity due to non-neutral monolayers may increase the instability of the film as it thickens [27]. This could be important in the case of LAO so that any processing-induced charged defects such as oxygen vacancy may play a role in charge compensation, hence affecting the film stability and growth mode transitions. Further experiments to understand this aspect would be useful.

4.2. Strain relaxation and buried layer

The compressive $SrRuO_3$ buried layer is not expected to contribute strain energy to drive crack formation in the tensile overlayer. Indeed, within the resolution of HXRD, we did not observe any change in the out-of-plane lattice parameter of $SrRuO_3$ regardless of the state (thickness, strain, or cracking) of the LAO overlayer, indicating a complete decoupling between the tensile overlayer and the compressive buried layer. The only exception was found in the thickest films (60 nm) where an abrupt expansion of the out-of-plane lattice parameter of the buried

layer was observed (see Ref. [23]), corresponding to a contraction of the in-plane lattice. This is indicative of the separation of the $SrRuO_3/SrTiO_3$ interface but not the $SrRuO_3$/LAO interface, which is possible if the crack penetrates through the LAO and $SrRuO_3$ layers to reach the substrate interface – a likely scenario in the thick film where the crack has enough driving force to overcome the closure force in the buried layer.

In contrast, the compressive buried layer can contribute strain energy to drive cross-hatch formation in the overlayer. This is evidenced by the decrease of the in-plane strain in the $SrRuO_3$ layer, shown in Figs. 9 and 10. Note that in Fig. 9b there is a coordinated strain relaxation in both the buried layer and the overlayer as the overlayer thickness increases (hence cross-hatch density increases). Indeed, the magnitude of strain relaxation in the two layers is comparable, which is reasonable if threading dislocations propagate through both layers to form misfit dislocations at the substrate interface. However, comparing Figs. 6 and 10 following a path pointing from the 2D/3D boundary into the 2D territory with increasing cross-hatching, we find an increasing strain relaxation in the buried layer is actually accompanied by an increasing compressive strain in the overlayer. In this case, the buried layer as an embedded "strain (relaxation) gauge" provides a more direct indicator than the overlayer, because the initial strain (before cross-hatch formation) in the buried layer is constant, whereas in the overlayer it varies with the deposition condition and increases as the growth condition enters further into the 2D territory.

A quantitative comparison of the predicted and observed critical conditions for cracking and cross-hatching is next made. In tensile LAO overlayers, cracking was observed at $\varepsilon = 1.4\%$ at a critical thickness between 2.5 and 5 nm. Assuming $\nu = 1/3$, $E = 250$ GPa [28] and $h_c = 5$ nm, Eq. (1) predicts $W_f = 0.98$ J m^{-2}, which is quite reasonable for a brittle oxide single crystal having no microstructure toughening. In compressive CZO/$SrRuO_3$ films, Fig. 9b indicates an unrelaxed overlayer strain of $\varepsilon_o = 2.5\%$ just before cross-hatching occurs at above 5 nm. Adding $\varepsilon_o h_o$ to the contribution of the buried layer of $h_b = 30$ nm at an unrelaxed strain of $\varepsilon_b = 0.6\%$, we predict according to Eq. (2) a critical h_o of 3.8 nm. This is slightly below the experimentally observed critical thickness. Such discrepancy is not surprising since these theoretical predictions are predicated on the propagation criteria and ignore the nucleation of threading dislocations, which would postpone strain relaxation.

On the other hand, cracking has little effect on the tensile strain in the LAO overlayer, and considerable compressive strain still exists in the CZO overlayer even with abundant cross-hatches. (In Fig. 9, the 30 nm film that retains about 80% of the initial strain has a cross-hatch spacing of 120 nm.) This indicates that strain relaxation by either mechanism is rather incomplete/inefficient. We believe the reason for this lies in the difficulty of nucleating additional cracks/dislocations in an increasingly smaller volume bounded by existing cracks/cross-hatches. For the same reason, the finest crack/cross-hatch spacing observed in our study was much coarser than theoretically predicted. For example, the finest crack spacing observed was about 500 nm in a 60 nm (1.4% strain) LAO film vs. the predicted minimum crack spacing of 16 nm [2] for such film if there is no nucleation barrier. Likewise, the finest cross-hatch spacing observed was about 120 nm in a 30 nm (2.0% strain) CZO film vs. the predicted minimum spacing of 15 nm [15].

The above discussion is most pertinent for overlayers grown in the 2D mode, which is the case for LAO overlayers that show cracking. Many CZO films near the 2D/3D boundary have considerably less strain than their counterparts deep in the 2D territory, but they developed cross-hatches nevertheless. Apparently, during deposition these films retain some 3D islands which contribute to strain relaxation [29,30]. Using the strain data of Fig. 6 (near the 2D/3D boundary), we found $\varepsilon_o = 1.8\%$ for the 20 nm film, giving a critical condition $h_o\varepsilon_o = 0.36$ nm which is higher than obtained from Fig. 9b, $h_o\varepsilon_o = 0.125$–0.25 nm. This discrepancy may be attributed to the slightly grainy microstructure of the films near the 2D/3D boundary, which would present additional obstacles for dislocation propagation.

5. Conclusions

1. $CaZrO_3$-based compressive overlayers with a theoretical 2.57% misfit deposited on $SrRuO_3/SrTiO_3$ substrates develop increasing strain as the growth mode become more 2D like. Beyond a critical condition well predicted by the prevailing theory, cross-hatches appear presumably by forming and propagating threading and misfit dislocations. The dislocations relieve strains not only in the CZO overlayer but also in the $SrRuO_3$ buried layer, by about the same magnitude. The cross-hatch pattern formed along the <100> directions is consistent with the <110> {110} slip system of perovskite.
2. $LaAlO_3$-based tensile overlayers with a theoretical 2.79% misfit deposited on $SrRuO_3/SrTiO_3$ substrates do not develop a significant strain unless they are grown under a high oxygen partial pressure. At larger thickness the 2D growth mode dominates, but the initial 5–10 monolayers contain small 3D islands. Larger islands formed at higher oxygen partial pressures are associated with higher tensile strains that are carried over to the thicker films growing past the 3D/2D transition. This eventually triggers cracking beyond a critical condition which is well predicted by the prevailing theory. The $SrRuO_3$ buried layer has no observable effect on strain relaxation or cracking of the overlayer.
3. Smooth crystalline overlayers without crack and cross-hatch can be obtained under the following conditions: medium temperature (550–600 °C) and pressure (0.1–20 mTorr) for $LaAlO_3$-based films; some 3D/2D transition conditions (e.g., 650 °C and 50 mTorr or 600 °C and 10–50 mTorr) for $CaZrO_3$-based films.

Please cite this article in press as: Wang Y et al., Control of strain relaxation in tensile and compressive oxide thin films, Acta Mater (2008), doi:10.1016/j.actamat.2008.07.010

Acknowledgments

This research was supported by the US National Science Foundation under Grant No. DMR-07-05054 (Electronic Materials) and DMR- 05-20020 (MRSEC).

References

[1] Setter N, Waser R. Acta Mater 2000;48:151.
[2] Thouless MD. J Am Ceram Soc 1990;73:2144.
[3] Beuth JL. Int J Solids Struct 1992;29:1657.
[4] Xia ZC, Hutchinson JW. J Mech Phys Solids 2000;48:1107.
[5] Chen SY, Chen IW. J Am Ceram Soc 1995;78:2929.
[6] Morito K, Suzuki T. J Appl Phys 2005;97:104107.
[7] Ernst F, Recnik A, Langjahr PA, Nellist PD, Ruhle M. Acta Mater 1998;47:183.
[8] Matthews JW, Blakeslee AE. J Cryst Growth 1974;27:118.
[9] Freund LB. MRS Bullet 1992;17:52.
[10] Mitchell TE, Heuer AH. Dislocations and mechanical properties of ceramics. In: Nabarro FRN, Hirth JP, editors. Dislocation in solids, vol. 12. New York: Elsevier; 2004. p. 75.
[11] Oh SH, Park CG. J Appl Phys 2004;95:4691.
[12] Sun HP, Tian W, Pan XQ, Haeni JH, Schlom DG. Appl Phys Lett 2004;84:3298.
[13] Kim SG, Wang Y, Chen IW. Appl Phys Lett 2006;89:031905.
[14] Thouless MD. Annu Rev Mater Sci 1995;25:69.
[15] Andrews AM, Speck JS, Romanov AE, Bobeth M, Pompe W. J Appl Phys 2002;91:1933.
[16] Williams AA, Thornton JMC, Macdonald JE, van Silfhout RG, van der Veen JF, Finney MS, et al. Phys Rev B 1991;43:5001.
[17] Geller S, Bala VB. Acta Crystallogr 1956;9:1019.
[18] Mathews MD, Mirza EB, Momin AC. J Mater Sci Lett 1991;10:305.
[19] García-Muñoz JL, Rodríguez-Carvajal J, Lacorre P, Torrance JB. Phys Rev B 1992;46:4414.
[20] Yamanaka S, Maekawa T, Muta H, Matsuda T, Kobayashi S, Kurosaki K. J Solid State Chem 2004;177:3484.
[21] Kawasaki M, Takahashi K, Maeda T, Tsuchiya R, Shinohara M, Ishiyama O, et al. Science 1994;266:1540.
[22] Koster G, Kropman BL, Rijnders G, Blank DHA, Rogalla H. Appl Phys Lett 1998;73:2920.
[23] Wang Y. Alloy perovskite oxide thin film as resistance switching non-volatile memory. Materials science and engineering. Philadelphia: University of Pennsylvania; 2008. 60.
[24] Freund LB. J Mech Phys Solids 1990;38:657.
[25] Rijnders G, Blank DHA, Choi J, Eom CB. Appl Phys Lett 2004;84:505.
[26] Kim DW, Kim DH, Kang BS, Noh TW, Lee DR, Lee KB. Appl Phys Lett 1999;74:2176.
[27] Noguera C. J Phys: Condens Mat 2000;12:R367.
[28] Belenky GL, Green SM, Roytburd A, Lobb CJ, Hagen SJ, Greene RL, et al. Phys Rev B 1991;44:10117.
[29] Herring C. J Appl Phys 1950;21:437.
[30] Coble RL. J Appl Phys 1963;34:1679.